Storm-Relative Winds and Helicity in the Tornadic Thunderstorm Environment

BRYNN W. KERR

NOAA/NWS Storm Prediction Center, Kansas City, Missouri

GRANT L. DARKOW

Department of Atmospheric Science, University of Missouri, Columbia, Missouri

(Manuscript received 31 October 1995, in final form 1 May 1996)

ABSTRACT

Environmental flow relative to tornado-producing thunderstorms is examined through the use of the large tornado proximity sounding dataset compiled at the University of Missouri. It is believed that the 184 soundings gleaned from this collection represent the largest, most restrictive database of its kind with observed storm velocities, as determined from microfilm of conventional National Weather Service radar. Using these storm velocities, mean storm-relative wind profiles were derived for the entire data sample and sample subsets based on tornadic intensity, strength of the mean environmental flow, magnitude of CAPE, and direction of storm motion with respect to the mean environmental wind vector. Although it is apparent that a number of tornadoes occur independent of the larger-scale flow, the mean storm-relative wind profiles suggest that there is a preferred storm-relative flow structure for tornadic thunderstorms. Tornadic intensity in association with this structure appears to strengthen as 1) the magnitude of storm-relative helicity grows through an increasingly deep layer of the lower through midtroposphere and 2) mid- and upper-level storm-relative winds strengthen while possessing decreasing directional variability at their respective heights above ground level (4–12 km AGL).

1. Introduction

Tornadoes have been observed to occur in association with a broad spectrum of convective storm types, both supercellular, characterized by ''deep, persistent'' mesocyclones, and nonsupercellular in nature (Doswell and Burgess 1993). While the destructive tornadic supercell has long been the focus of the research community (e.g., Browning 1964; Lemon and Doswell 1979; Klemp 1987), other studies have acknowledged the generally weaker, but occasionally quite damaging, nonsupercell tornadic storm (e.g., Wakimoto and Wilson 1989).

Although many questions with regard to the development and evolution of tornadoes remain unresolved, much has been learned about the storm-scale processes leading to tornadogenesis since the Thunderstorm Project (Byers and Braham 1949), the first comprehensive investigation of ''ordinary'' deep, moist convection. This study established the concept of the thunderstorm cell as the basic convective circulation, which evolves through a characteristic life cycle from initial cumulus development through storm maturity and dissipation. Of particular significance, Byers and Braham noted the role of vertical wind shear in sustaining convection that is strong enough to overcome the initially inhibitive effects of shear.

In pioneering studies of rawinsonde data antecedent to tornadic storms, Fawbush and Miller (1954) and Beebe (1955) linked the thermodynamic and kinematic structure of the environment to the character of ensuing convection and associated tornadoes. Several decades later, numerical cloud modeling research substantiated this relationship (Weisman and Klemp 1982, 1984, 1986). While the degree of thermodynamic instability is essential to updraft strength, Weisman and Klemp suggested that it is the environmental shear profile (i.e., the shape and magnitude of the hodograph) that is most critical to storm structure and sustenance. Theoretically, this has been explained by the dynamic interaction between the storm and the environmental flow relative to it, which, with the ''proper'' hodograph,[1] promotes systematic updraft regeneration on a preferred storm flank (Newton and Newton 1959; Rotunno and

Corresponding author address: Brynn W. Kerr, NOAA/NWS Storm Prediction Center, Federal Office Building, Room 1728, 601 E. 12th Street, Kansas City, MO 64106.
E-mail: Brynn.W.Kerrnoaa.gov

[1] Note that the hodograph is not affected by a transformation from the environmental reference frame to the storm-relative reference frame.

Klemp 1982) and the development of storm rotation (Rotunno 1981; Davies-Jones 1984; Lilly 1986b).

Reminiscent of the studies of Fawbush and Miller (1954) and Beebe (1955), Maddox (1976) and Darkow and McCann (1977) used tornado proximity sounding data to examine environmental storm-relative flow. While Maddox generated mean storm-relative wind profiles from composited environmental wind profiles and an assumed storm velocity, Darkow and McCann offered an alternative compositing technique, utilizing storm velocities as determined from microfilm of conventional National Weather Service radar. Both studies showed that, for the typical tornadic thunderstorm, flow approaches the updraft to the right of its motion before veering with height to the rear of the updraft in the upper troposphere, with a relative minimum in speeds at midtropospheric levels (see Fig. 1). They also revealed similarities in storm-relative flow between various subclassifications of tornado-producing thunderstorms, while the environmental flow exhibited marked variability.

Drawing on the work of Darkow and McCann (1977), among many others, Lemon and Doswell (1979) proposed a three-dimensional conceptual model of the tornadic ''supercell,'' illustrating the relationship between storm structure and the environmental storm-relative flow (Fig. 2). Integration of observational and modeling findings suggests the following: Strong low-level storm-relative winds feed buoyant air into an updraft that is amplified and sustained by its own rotation and high helicity (Lilly 1986a,b), derived from the tilting and stretching of streamwise vorticity associated with the vertical shear of the ambient flow (Rotunno 1981; Davies-Jones 1984; Rotunno and Klemp 1985). Storm-scale rotation is most pronounced at midtropospheric levels of the updraft until processes are able to induce low-level mesocyclone development prior to tornadogenesis (Klemp and Rotunno 1983; Davies-Jones and Brooks 1993).

According to Klemp and Rotunno (1983), the low-level mesocyclone amplifies in response to the entrainment, tilting, and stretching (by the updraft) of vorticity along the leading edge of the *forward flank* downdraft outflow. Although Klemp and Rotunno emphasized the baroclinic contribution, this vorticity is intensified by stretching associated with convergence along the outflow boundary. The magnitude of both contributors is to a large extent determined by the momentum of the storm-relative flow, as well as the potential negative buoyancy of mid- and upper-tropospheric air entrained into the downdraft.

Meanwhile, Davies-Jones and Brooks (1993) argued that it is the baroclinically generated cyclonic vorticity associated with the thermal gradient between the updraft and the evaporatively cooled *rear flank* downdraft that leads to the development of the low-level meso-
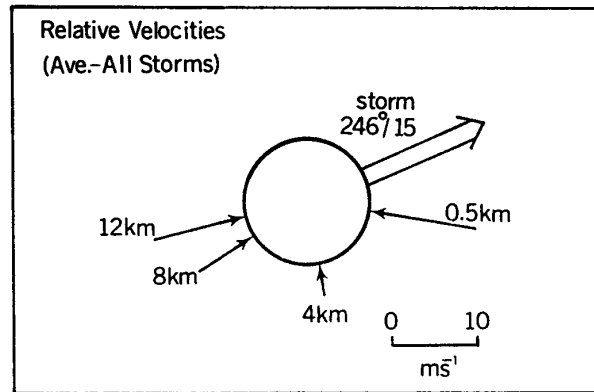

FIG. 1. Mean storm-relative wind profile for the 121 tornadic thunderstorms composing Darkow and McCann's dataset. The open circle represents the updraft core, with storm motion depicted by broad arrow. Storm-relative wind vectors 0.5, 4, 8, and 12 km above ground level are shown (from Darkow and McCann 1977).

cyclone, as it is entrained and stretched by the updraft. Brooks et al. (1994a) explained further that the success of this process is ultimately linked to the relationship between the strength of the mid- to upper-level storm-relative flow and the resultant distribution of precipitation relative to the mesocyclone.

While the influence of environmental storm-relative flow on storm structure and dynamics appears to be critical in supercell (mesocyclonic) tornadogenesis, Carbone (1983) provided evidence that tornadogenesis may not always be so dependent on the larger-scale environment. This was further supported by Wilson (1986) and Wakimoto and Wilson (1989), who observed that interacting surface boundaries or convergence zones may produce localized low-level shear and thermodynamic conditions similar to those associated with supercells, even in the presence of weak environmental vertical shear.

In light of the preceding discussion, the purpose of the current study is to reexamine and expand upon the work of Darkow and McCann (1977) by 1) using a larger data sample and 2) exploring some of the more contemporary parameters considered to be critical to the development and evolution of tornadic thunderstorms.

2. Data source and methodology

The database for this study is the University of Missouri tornado proximity sounding collection, gathered over the 20-yr period from 1965 to 1984, using Darkow's (1969) screening criteria as follows: 1) the tornado must have occurred between 15 min prior to and 105 min after rawinsonde release time, 2) the tornado must have occurred within 50 statute miles of the re-
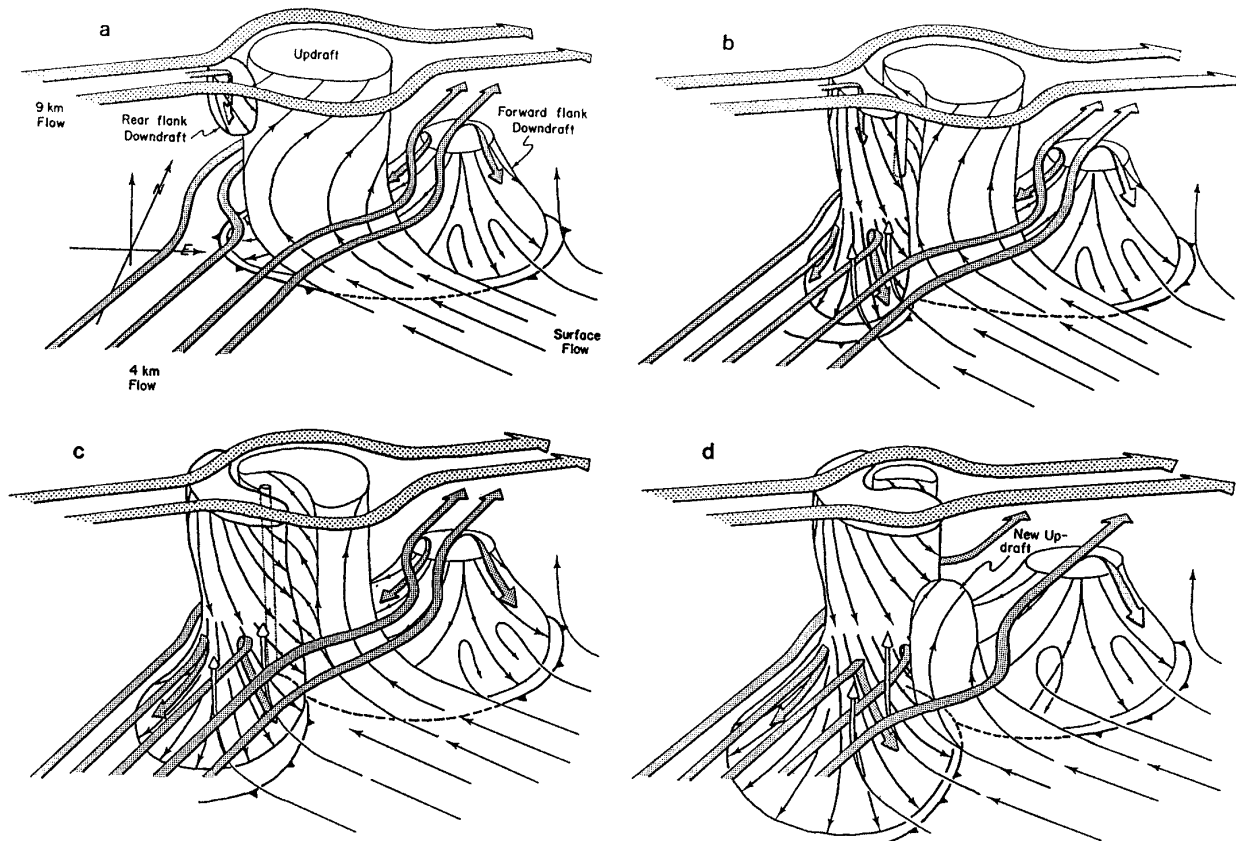
FIG. 2. Schematic three-dimensional depiction of evolution of the drafts, tornado, and mesocyclone in an evolving supercell storm. The stippled flow line suggesting descent of air from the 9-km stagnation point has been omitted from (c) and (d) for simplicity. Flow lines throughout the figure are storm-relative and conceptual only, and are not intended to represent flux, streamlines, or trajectories (from Lemon and Doswell 1979).

lease site, and 3) the rawinsonde release must have taken place in the airmass that produced the tornadic storm (i.e., any postfrontal- or outflow-affected soundings were purged from the collection).[2] From this collection, 184 cases were found to have radar microfilm suitable for detecting storm motion, increasing Darkow and McCann's (1977) sample size by 50%.

With the exception of one case in the Pacific Northwest, the tornado proximity soundings in this database encompassed 21 states east of the Rockies (Fig. 3). While a majority of these were from the Plains states, a large number came from the Gulf Coast states, the middle Mississippi and Ohio River Valleys, and the Great Lakes region, with a few

from the mid-Atlantic states. Every month of the year was represented in the database, although most cases were from the late spring and early summer months. The F-scale (Fujita 1971) frequency distribution of this dataset is shown in Fig. 4 and compares favorably with the long-term F-scale frequency distribution for all tornado occurrences as compiled by the National Severe Storm Forecast Center (Ostby 1993).

Storm-relative wind profiles for each proximity sounding were generated in the following manner. Environmental winds were interpolated from the original standard pressure levels at 50-mb increments (as obtained from the National Climatic Data Center) to values at 1-km increments above ground level (AGL) from the surface to 15 km AGL, (unless noted otherwise, all heights from this point on are AGL) with the 0.5-km level also computed in an attempt to retain some boundary layer features. Parent storm velocities were determined by averaging three 30-min displacements of the most intense portion of

---

[2] Even with such strict limitations placed on the definition of "proximity" sounding, Brooks et al. (1994b) pointed out that we still cannot be completely certain that a rawinsonde sampled the actual tornadic thunderstorm environment, due to the subsynoptic-scale variability often observed in convective environments.
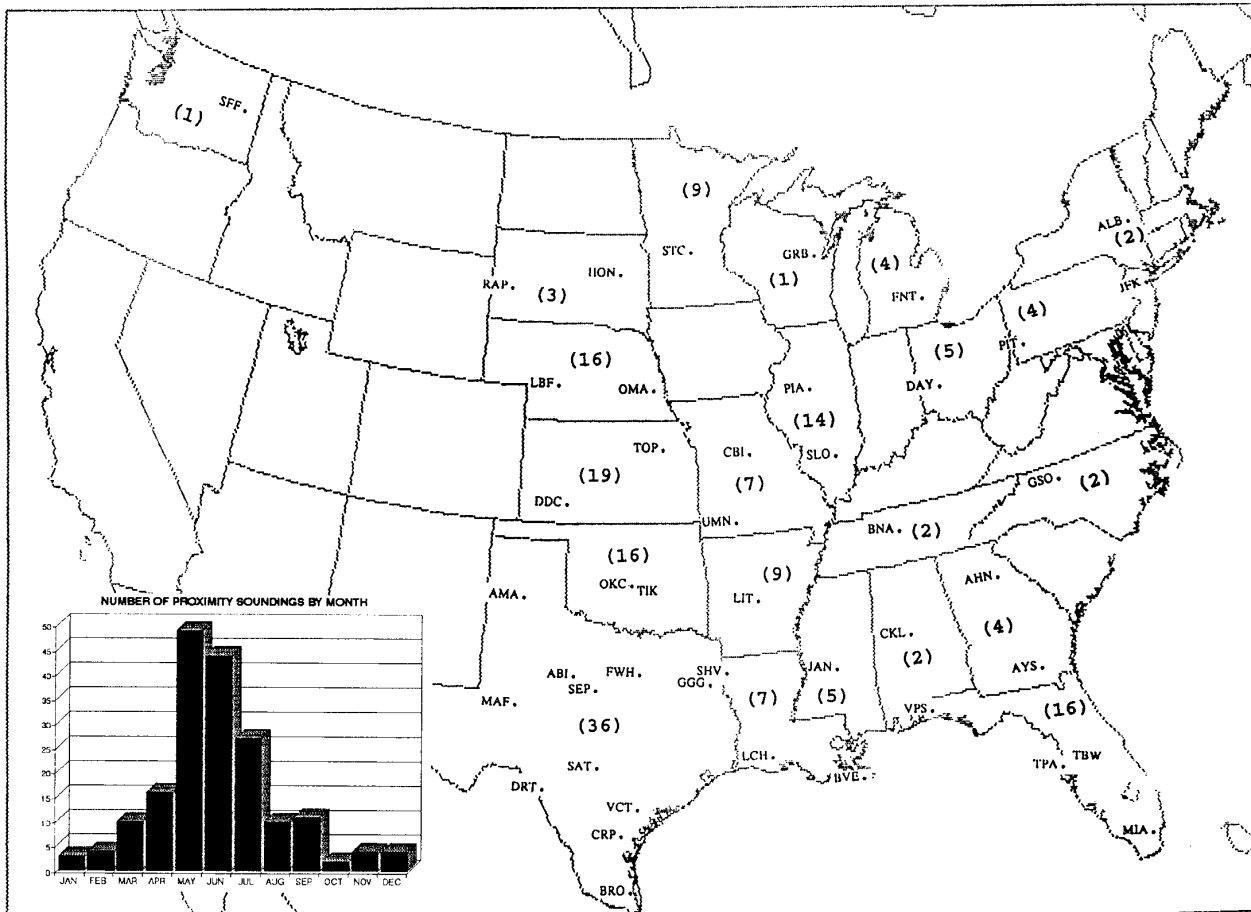
FIG. 3. Geographic and temporal distributions of the 184 tornado proximity soundings analyzed in this study. Numbers in parentheses represent total occurrences by state, with rawinsonde sites depicted by appropriate three-letter station identifiers.

the radar echo (or echo centroid when this was not possible), with the middle 30-min period centered on tornado time and weighted twice as heavily as the other periods. Storm velocities were then subtracted from the environmental winds at each of the aforementioned heights to obtain the storm-relative winds.

One dilemma in providing meaningful composites of wind data, storm-relative or environmental, is illustrated in Fig. 5. Shown in Figs. 5a and 5b are storm-relative wind profiles for two storms moving in opposite directions, one (Fig. 5b) with a magnitude slightly greater than the other (Fig. 5a). With respect to the storm motion vector, the low-, mid-, and upper-level winds (represented by L, M, and H, respectively) approach from the same direction and are identical in magnitude. However, simple vector averaging of the winds and storm velocities yields that shown in Fig. 5c. Mean storm-relative flow is *calm,* clearly unrepresentative of either profile. One

may overcome this difficulty by vectorially averaging after first rotating the individual storm velocities to the direction of the sample mean storm velocity vector (Darkow and McCann 1977). Rotating Fig. 5a by 180° before averaging with Fig. 5b (which in this case does not need to be rotated) yields the more representative mean storm-relative wind profile shown in Fig. 5d.

Even after compositing in the manner of Darkow and McCann (1977), cancellation inherently associated with the vector-averaging process remains a problem. Obviously, for a particular level, storm-relative winds do not approach from the same direction at the same speed for all storms, as in the previous example. Taking this into account, composites of storm-relative wind profiles for the total sample and various subsets in this study were generated as in the example above, except that the magnitude of the mean storm-relative winds at each level were computed via scalar averaging.
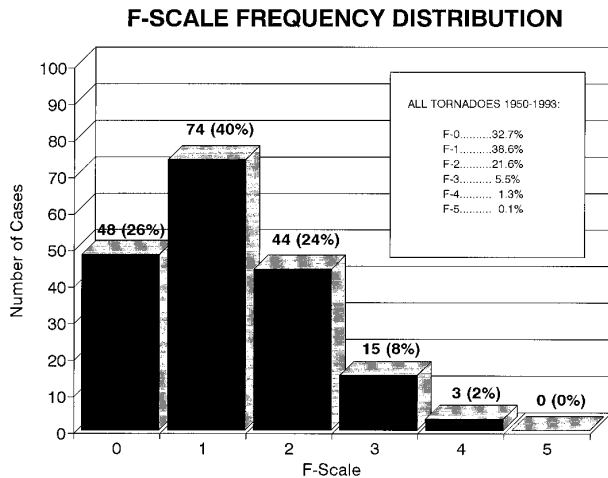
F-SCALE FREQUENCY DISTRIBUTION

FIG. 4. F-scale frequency distribution of the 184 tornadic storms composing the database in this study. Numbers in parentheses represent the percentage of the total sample. Frequency distribution by F-scale intensity for all tornado occurrences compiled by the National Severe Storm Forecast Center between 1950 and 1993 is shown in the inset.

3. Results

a. Mean profile for the entire proximity collection

Displayed in Fig. 6 is the mean storm-relative wind profile for the 184 proximity soundings composing the dataset used in this study. With a mean motion to the east-northeast, these storms average 13° to the right of the mean wind direction (as shown next to ''Deviate motion''), at 91% of the mean wind speed,[3] in environments with a mean convective available potential energy (CAPE) of 1421 J kg^{-1}. Possessing a mean storm-relative helicity of 142 m^2 s^{-2} (0–3 km), and a classically veering profile from the lower levels into the upper troposphere on the right flank of the storm, the mean storm-relative flow structure is consistent with conceptual models commonly associated with tornadic supercells.

When the magnitudes of the storm-relative winds in Fig. 6 are compared to those in Fig. 1, speeds of 12–15 m s^{-1} in the lowest 1 km are quite similar to those found by Darkow and McCann (1977), as is the minimum in relative flow in the 2–4-km layer. However, speeds above 2 km (e.g., as shown in Fig. 6, 8–9 m s^{-1} in the 2–4-km layer and 18–20 m s^{-1} in the 10–12-km layer) are roughly twice the magnitude found by

Darkow and McCann. This discrepancy is attributed to the variability of the mid- and upper-level storm-relative wind directions, which leads to significant cancellation of storm-relative wind magnitude when employing the vector-averaging technique used by Darkow and McCann.

Frequency distributions of individual storm-relative wind directional deviations from their respective sample mean storm-relative wind at the 0.5-, 4-, 7-, and 12-km levels are shown in Fig. 7. The least amount of variability is observed in the low-level inflow layer, where 80% of the 0.5-km storm-relative winds are within 40° of the 0.5-km-mean storm-relative wind direction. Only 40%–50% of the storm-relative winds at 4, 7, and 12 km are within 40% of the mean storm-relative wind direction at their respective levels in the mid- and upper troposphere. The frequency distribution for storm-relative wind speeds at 4 km (not shown) suggests that the stronger mean midtropospheric storm-relative wind speeds computed in this study are not the by-product of a small number of high wind speeds biasing the average.

A scatter diagram of CAPE versus storm-relative helicity for the proximity soundings in this dataset is displayed in Fig. 8. Storm-relative helicity was computed after Davies-Jones et al. (1990), while CAPE was obtained by lifting a parcel with the mean thermodynamic properties of the lowest 0.5-km layer. Figure 8 illustrates the broad range of environmental conditions in which tornadic storms occur, a finding noted previously by Maddox (1976) and Johns et al. (1992), among others. A considerable number of the tornadoes appear to be associated with nonmesocyclonic convection, as nearly one-third of the data sample (55 cases, including 8 cases with tornado intensity ratings of F-2 or greater) possesses storm-relative helicity ranging from −50 m^2 s^{-2} to 50 m^2 s^{-2}, suggesting minimal midlevel updraft rotation. Furthermore, a number of soundings possess both weak CAPE and low storm-relative helicity values, similar to those environments examined by Wakimoto and Wilson (1989) for nonsupercellular tornadic storms near Denver, Colorado.

b. F-scale subsets

Mean storm-relative wind profiles arrayed according to F-scale intensity are presented in Fig. 9. The most obvious difference among these subsets lies in the strength of the storm-relative winds in the boundary layer (0–1 km), as speeds increase steadily with increasing F-scale intensity. Somewhat less discernable is the gradual strengthening of speeds and increasing degree of veering through the lowest several kilometers. This is quantified in Figs. 10a–c, which illustrate how storm-relative helicity values increase with increasing F-scale intensities. While much of the 0–3-km-layer storm-relative helicity for each subset is pos-

---

[3] The mean environmental wind for each individual sounding was computed by vectorially averaging the winds from the surface to 12 km. This is essentially the same layer used by Darkow and McCann (1977) and Maddox (1976), and is used to represent the cloud-bearing layer.
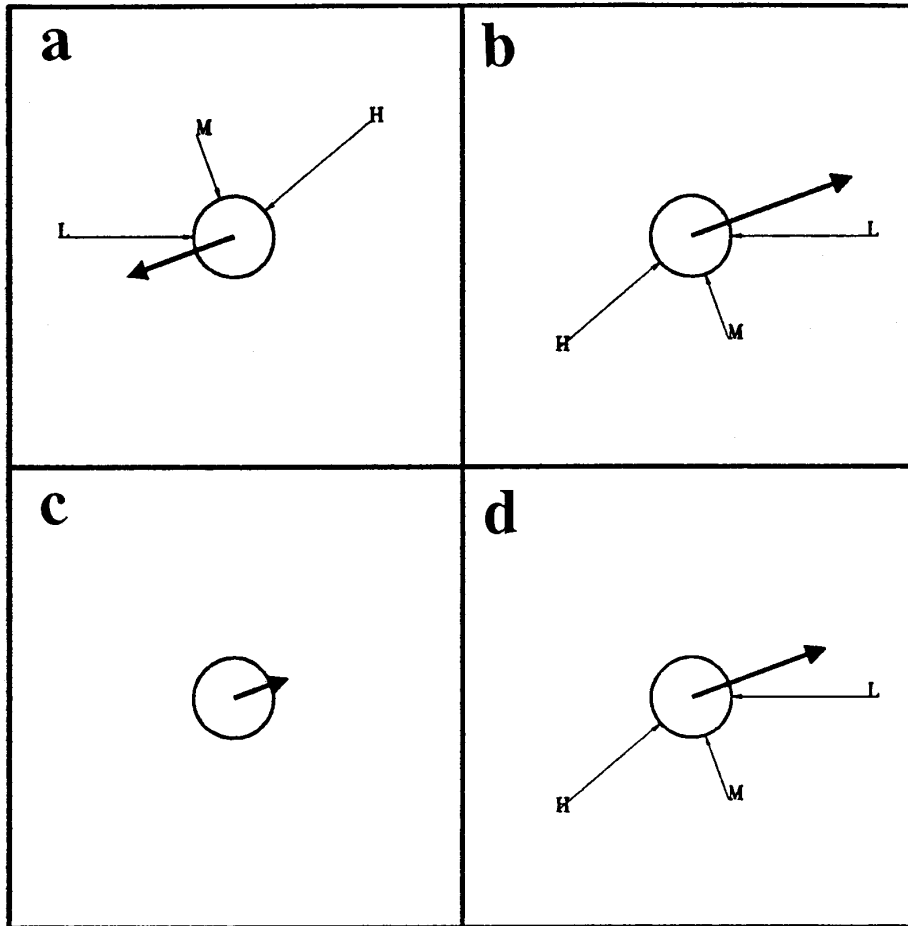
FIG. 5. (a) and (b) Schematic of hypothetical storm-relative wind profiles for two storms, with storm motions represented by thick black arrows. Storm motion for ''a'' is from 70°, while storm motion for ''b'' is from 250°, with ''b'' greater in magnitude than ''a.'' Storm-relative winds at low, mid-, and high levels are represented by L, M, and H, respectively, and, with respect to storm motion, approach from the same direction at the same magnitude for both ''a'' and ''b.'' (c) Simple vector average of storm-relative winds and storm motions in (a) and (b). Mean storm motion is represented by thick black arrow with a direction from 250°, while mean storm-relative winds are calm. (d) Simple vector average of storm-relative winds after first rotating storm motion vector and storm-relative wind vectors for ''a'' and ''b'' by an amount equivalent to the difference between the direction of the respective storm motion vector and the sample mean storm motion vector (180° for ''a''; 0° for ''b'').

sessed in the boundary layer flow, values indicate a trend toward increasing storm-relative helicity with tornadic intensity in the layers above.[4]

Although Darkow and McCann (1977) found that storm-relative wind speeds increased at all levels with increasing F-scale intensity, Figs. 9a–d suggest that

this relationship is not quite so clear cut. Mid- and upper-level storm-relative wind speeds and, to a large extent, directions are quite similar for F-0 through F-2 tornadic thunderstorms. Given similar CAPE in the environment of these storms (Fig. 10d), this appears to suggest that the intensity of the tornado is directly proportional to the strength of the storm-relative helicity, a relationship implied by Davies-Jones et al. (1990).

However, Fig. 9d displays noticeably stronger mid- and upper-level storm-relative flow (5–12 km) for the F-3 and F-4 tornadoes. If one concedes that these strong and violent tornadoes are all likely associated with

---

[4] It is acknowledged that interpretation of the results for the F-scale subsets may be subject to some question, given the inherent statistical uncertainties associated with the small sample sizes of the F-3 and F-4 subsets.
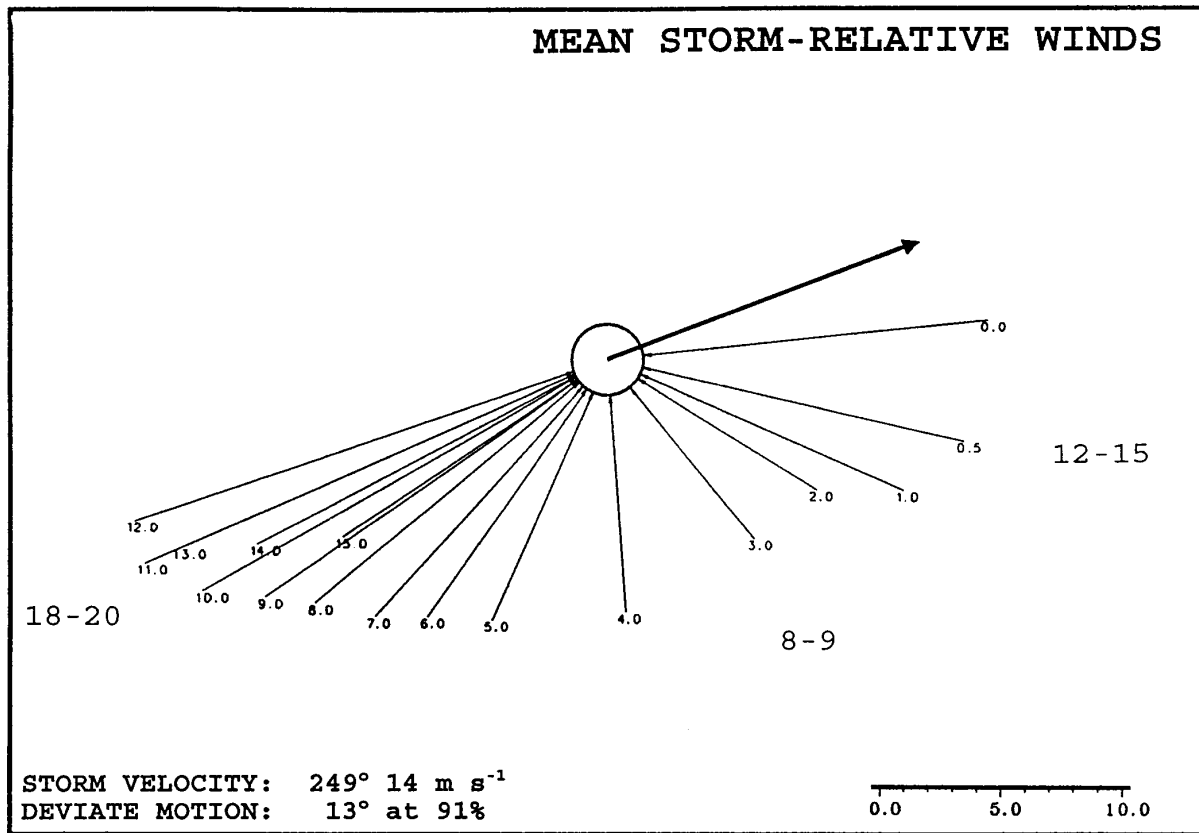
FIG. 6. Mean storm-relative wind profile for the 184 tornadic thunderstorms composing the dataset in this study. The open circle represents the updraft core, with the mean storm velocity represented by the thick arrow. Storm-relative wind vectors for the surface (0.0), 0.5, 1.0, 2.0, ..., 15.0 km AGL are shown. Range of speeds in m s^{-1} (scale in lower-right corner) for the surface to 1.0-km, 2.0–4.0-km, and 10.0–12.0-km layers are shown next to the appropriate vectors.

deep, persistent mesocyclones (Doswell and Burgess 1993), the incremental difference between the F-2 subset and the higher F-scale intensity subset (note, also, the mean CAPE values in Fig. 10d) suggests that a large number of F-2 tornadoes in this dataset are associated with nonsupercellular convection (recall discussion related to Fig. 8 in section 3a). This would then lead one to infer that, in order to discriminate nonsupercell and supercell environments associated with weaker tornadoes from those supercell environments associated with particularly strong or violent tornadoes, it is essential to consider the strength of the mid- and upper-level storm-relative flow in addition to storm-relative helicity.

One explanation of the physical relevance of these parameters has been provided by Brooks et al. (1994a,b) through numerical modeling and analysis of proximity soundings. They found evidence suggesting that a balance between the strength of the mid-level storm-relative winds and the mid-level mesocyclone (a function of storm-relative helicity) is necessary for the genesis of long-lived low-level mesocyclones, as both act to horizontally redistribute precipitation about the updraft and are thus instrumental in the baroclinic generation of low-level vorticity. Their numerical simulations indicated that if the midlevel storm-relative flow is too weak relative to the strength of the midlevel mesocyclone, and therefore the bulk of the precipitation falls near the updraft, low-level mesocyclogenesis is rapid, but short lived, as rain-cooled downdrafts quickly cut off storm inflow. Interference from outflow is slower to occur if precipitation is blown farther away from the updraft by stronger midlevel storm-relative winds. If this displacement is too great, however, baroclinic generation of low-level vorticity may not be sufficient to support low-level mesocyclogenesis.

c. Magnitude of the mean environmental flow

Unlike the mean storm-relative wind profiles, mean environmental wind profiles for the F-scale subsets (not shown) are consistent with those of Darkow and
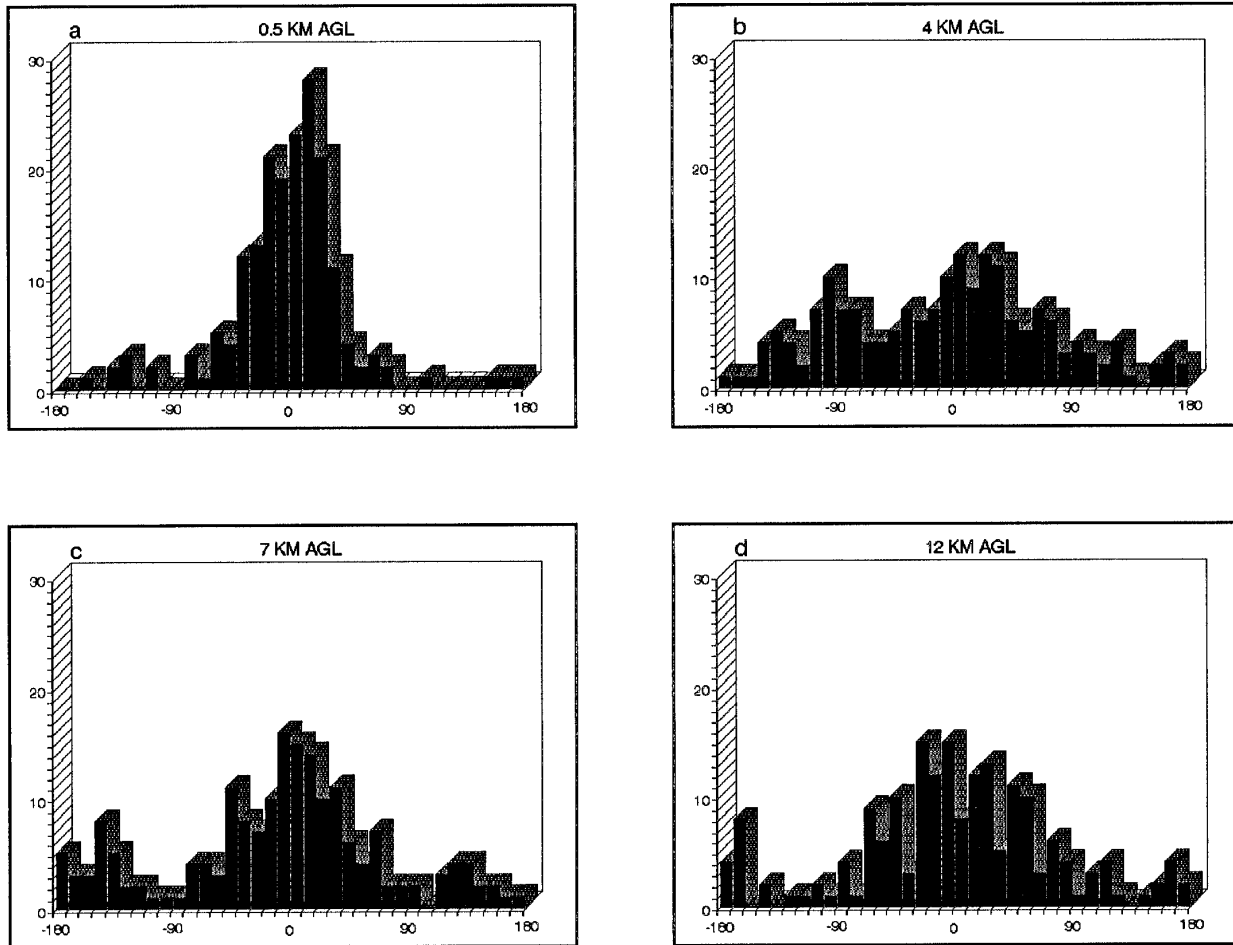
FIG. 7. Frequency distributions of individual storm-relative wind directional deviations from the sample mean storm-relative wind at (a) 0.5, (b) 4, (c) 7, and (d) 12 km AGL. Positive (negative) values are to the right (left) of the respective mean storm-relative wind vectors.

McCann (1977), displaying a systematic increase in environmental wind speeds at all levels with increasing F-scale intensity. Pursuing this relationship further, the dataset was subdivided according to the magnitude of the mean environmental wind vector of each sounding. Mean storm-relative wind profiles for these subsets are displayed in Fig. 11, while mean storm-relative helicity and CAPE are presented in Fig. 12.

Perhaps not surprisingly, the mean F-scale intensities for each subset increase steadily with the magnitude of the mean environmental flow (see Table 1), possessing values that range from 0.6 for the 10 m s^{-1} or less subset to 1.9 for the greater than 30 m s^{-1} subset. Of the 18 F-3 and F-4 tornadic storms, 3 fell in the 11–20 m s^{-1} subset (composing nearly 5% of the subset sample), with 10 in the 21–30 m s^{-1} subset (15% of the subset sample) and 5 in the greater than 30 m s^{-1} subset (21% of the subset sample).

All but 3 of the 29 cases in the 10 m s^{-1} or less subset were F-0 or F-1 intensity tornadoes. For this subset, the mean storm-relative wind profile (Fig. 11a) is consistent with nonsupercellular (nonmesocyclonic) convection that is significantly influenced by mesoscale features such as outflow boundaries and sea breezes (14 of the tornadic storms occurred near Tampa, Florida, or in the vicinity of the Gulf Coast). Storm motions deviate strongly from the mean wind direction at speeds greater than the mean wind speed. Storm-relative winds tend to approach the front flank at all levels and are rather weak (averaging 8 m s^{-1} or less) in magnitude through the lowest several kilometers, with almost negligible storm-relative helicity (Figs. 12a–c).

As the magnitude of the mean environmental flow strengthens, not only does the average F-scale intensity increase, but mean storm-relative wind profiles
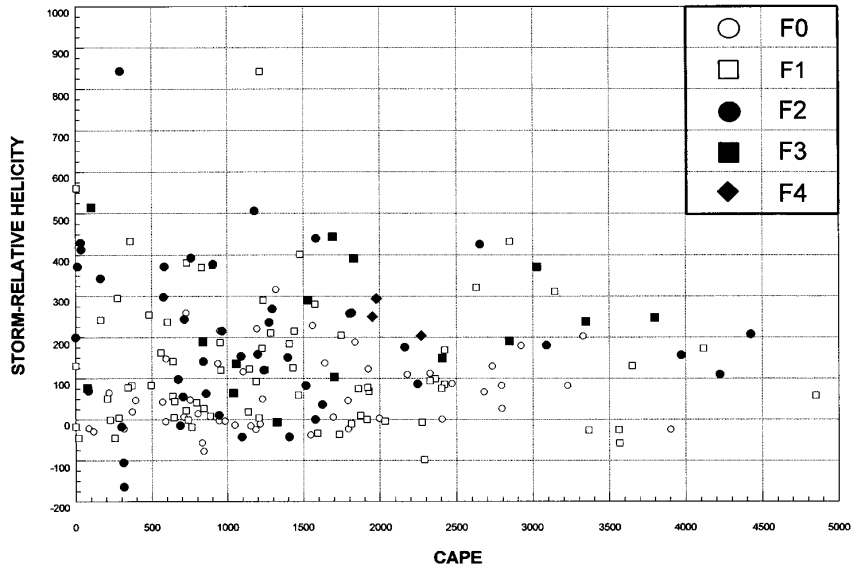
FIG. 8. Scatter diagram of CAPE (J kg^{-1}) vs 0–3-km storm-relative helicity (m^2 s^{-2}), as computed from the 184 tornado proximity soundings and storm velocities composing the dataset in this study.
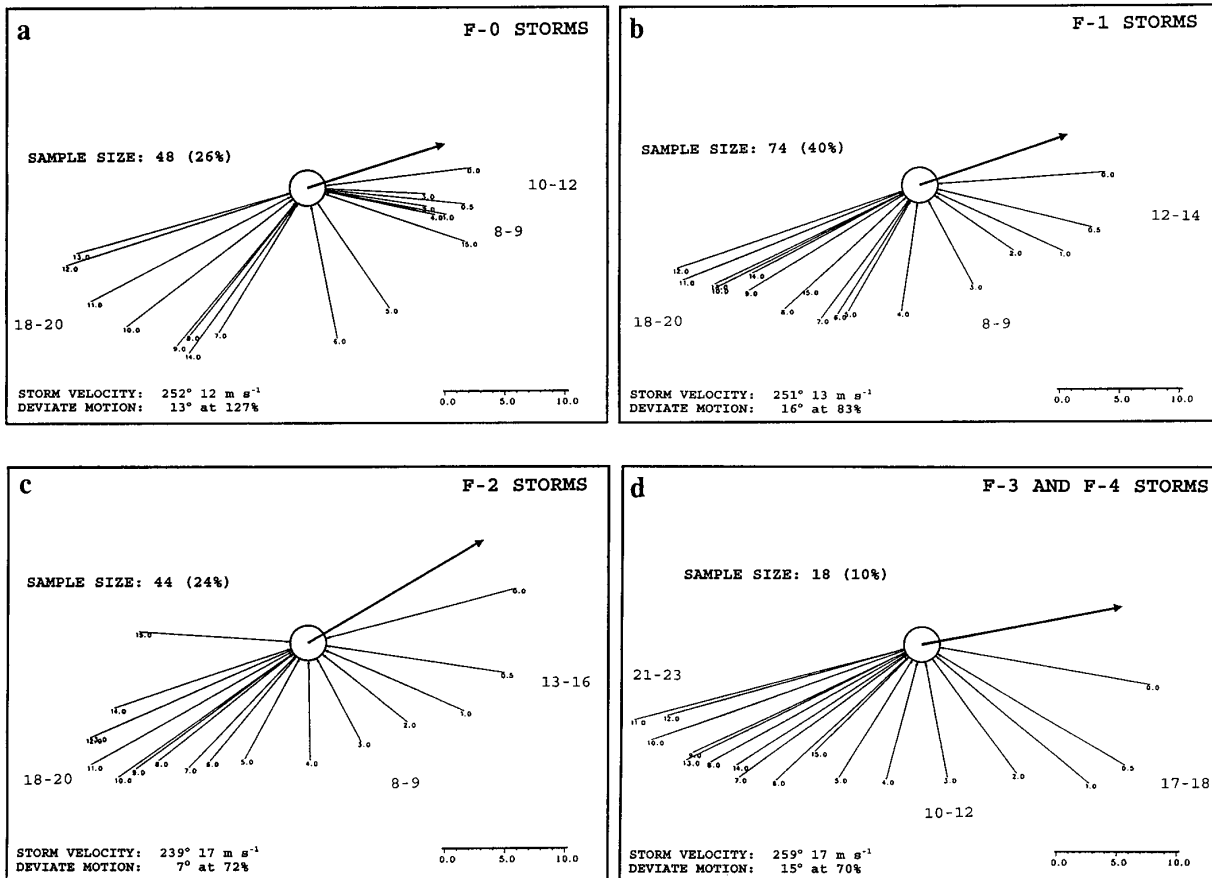

FIG. 9. As in Fig. 6 except for (a) F-0 subset, (b) F-1 subset, (c) F-2 subset, and (d) F-3 and F-4 subset.
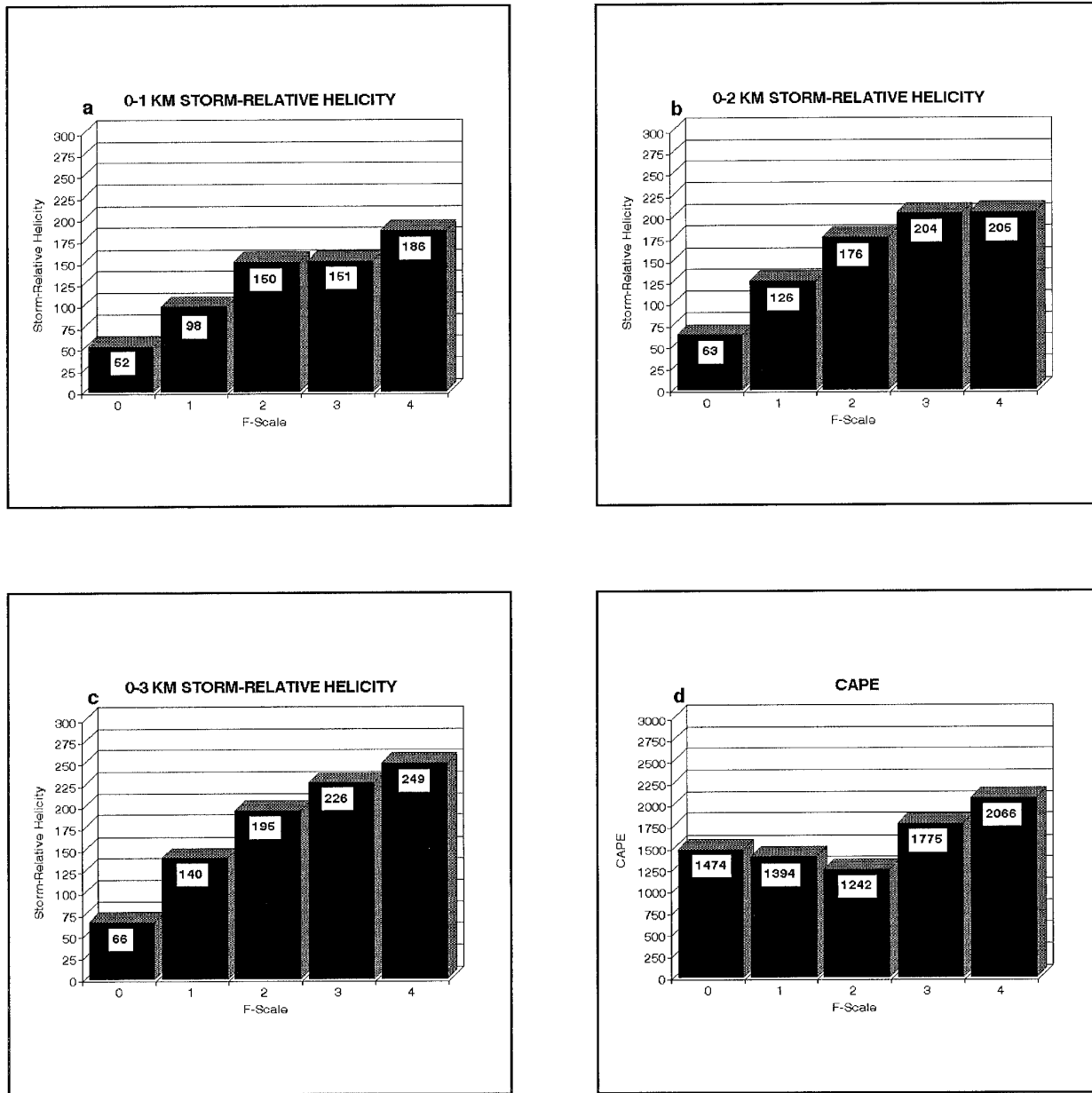
FIG. 10. Mean storm-relative helicity values ($m^2\ s^{-2}$) for the F-scale subsets in the (a) 0–1-km layer, (b) 0–2-km layer, and (c) 0–3-km layer. (d) Mean CAPE values ($J\ kg^{-1}$) for the F-scale subsets.

(Figs. 11b–c) appear to become more organized and consistent with supercellular (mesocyclonic) convection. In the lowest several kilometers, storm-relative winds increase in magnitude and display greater veering with height. This is reflected in Figs. 12a–c, which suggest a particularly dramatic increase in mean storm-relative helicity (and implied updraft rotation) as mean environmental winds strengthen from 11–20 m s^{-1} to 21–30 m s^{-1}. In mid- and up-

per levels, storm-relative winds also increase in speed with strengthening environmental flow while at the same time possessing substantially less directional variability (Table 1). The percentage of storm-relative winds within 40° of the subset mean storm-relative wind direction nearly triples from the 11–20 m s^{-1} subset to the greater than 30 m s^{-1} subset at the 4-km level, while the percentage nearly doubles at both the 7- and 12-km levels.
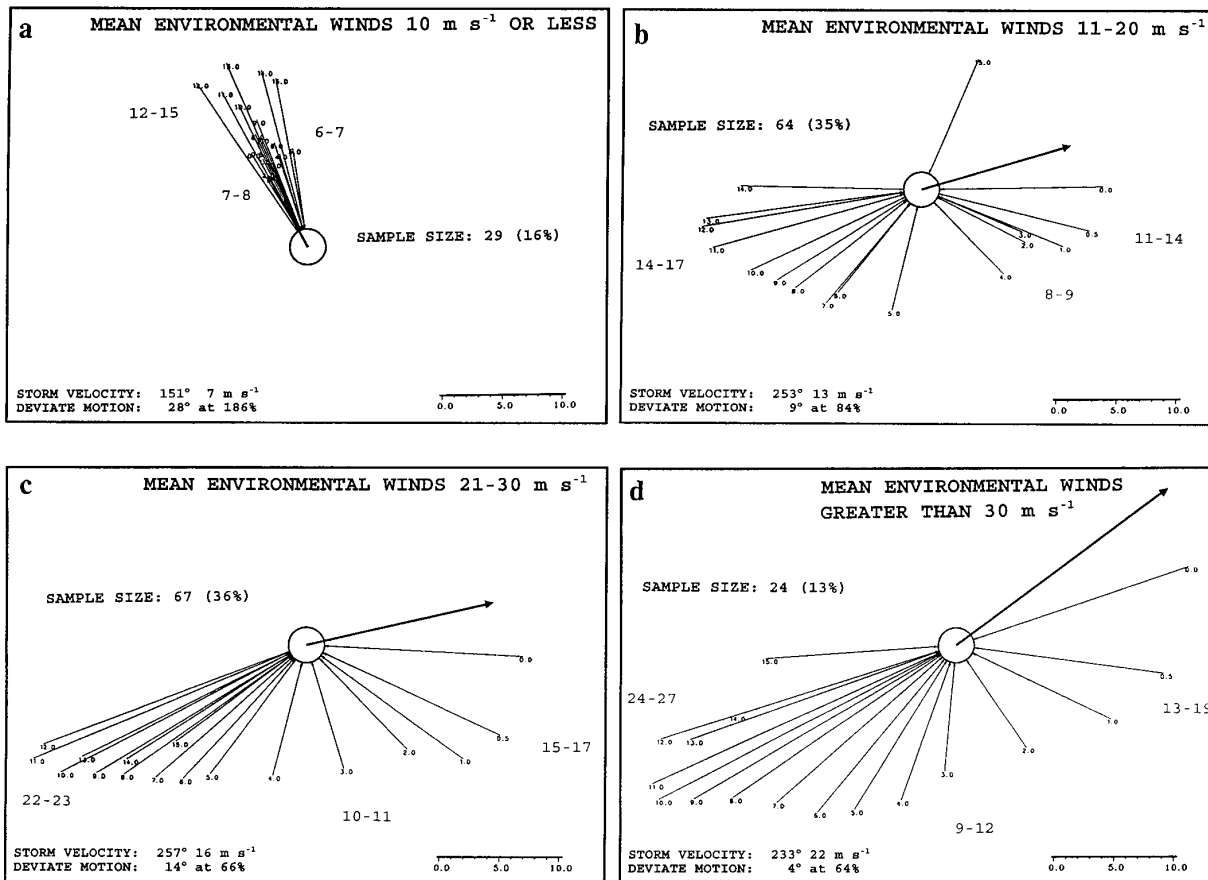
FIG. 11. As in Fig. 6 except for (a) 10 m s^{-1} or less subset, (b) 11–20 m s^{-1} subset, (c) 21–30 m s^{-1} subset, and (d) greater than 30 m s^{-1} subset.

d. CAPE subsets

Both the F-scale subsets and the mean environmental wind subsets suggest a positive relationship between the magnitude and shear of the environmental flow, the strength and orientation of the storm-relative winds, and the tornadic intensity. However, Figs. 10d and 12d indicate that the relationship between environmental instability and tornadic intensity is somewhat dubious. While mean CAPE values tend to increase with increasing F-scale intensity (and stronger mean environmental flow) in Fig. 10d, they generally decrease with increasingly strong mean environmental flow (and stronger F-scale intensity) in Fig. 12d.

Isolating CAPE, mean storm-relative wind profiles were derived for environments with weak (less than 1000 J kg^{-1}), moderate (1000–2500 J kg^{-1}), and high (greater than 2500 J kg^{-1}) instability, as shown in Fig. 13. Readily apparent is the striking similarity among the three profiles. Mean storm-relative helic-

ity possessed by the low-level flow approaching the right-front quadrant of the storm in the high CAPE subset is 161 m^2 s^{-2}, only slightly greater than that possessed by the weak and moderate CAPE subsets (147 m^2 s^{-2} and 132 m^2 s^{-2}, respectively), owing to the slightly greater mean strength of the storm-relative winds in the boundary layer. Otherwise, differences in the magnitude and direction of the mean mid- and upper-level flows appear negligible. Mid-level winds (2–4 km) approach the storm nearly perpendicular to, and to the right of, its motion at speeds of 8–10 m s^{-1}, while upper-level winds (10–12 km) impinge on the rear of the storm at speeds of 17–20 m s^{-1}. Given the similarities in the storm-relative flow structure, it is not surprising to find that the mean F-scale intensities for the three subsets are also comparable, with values of 1.1, 1.3, and 1.2 for the weak, moderate, and high CAPE subsets, respectively.

Thus, it appears that tornadic intensity is not dependent on CAPE. This conclusion is supported
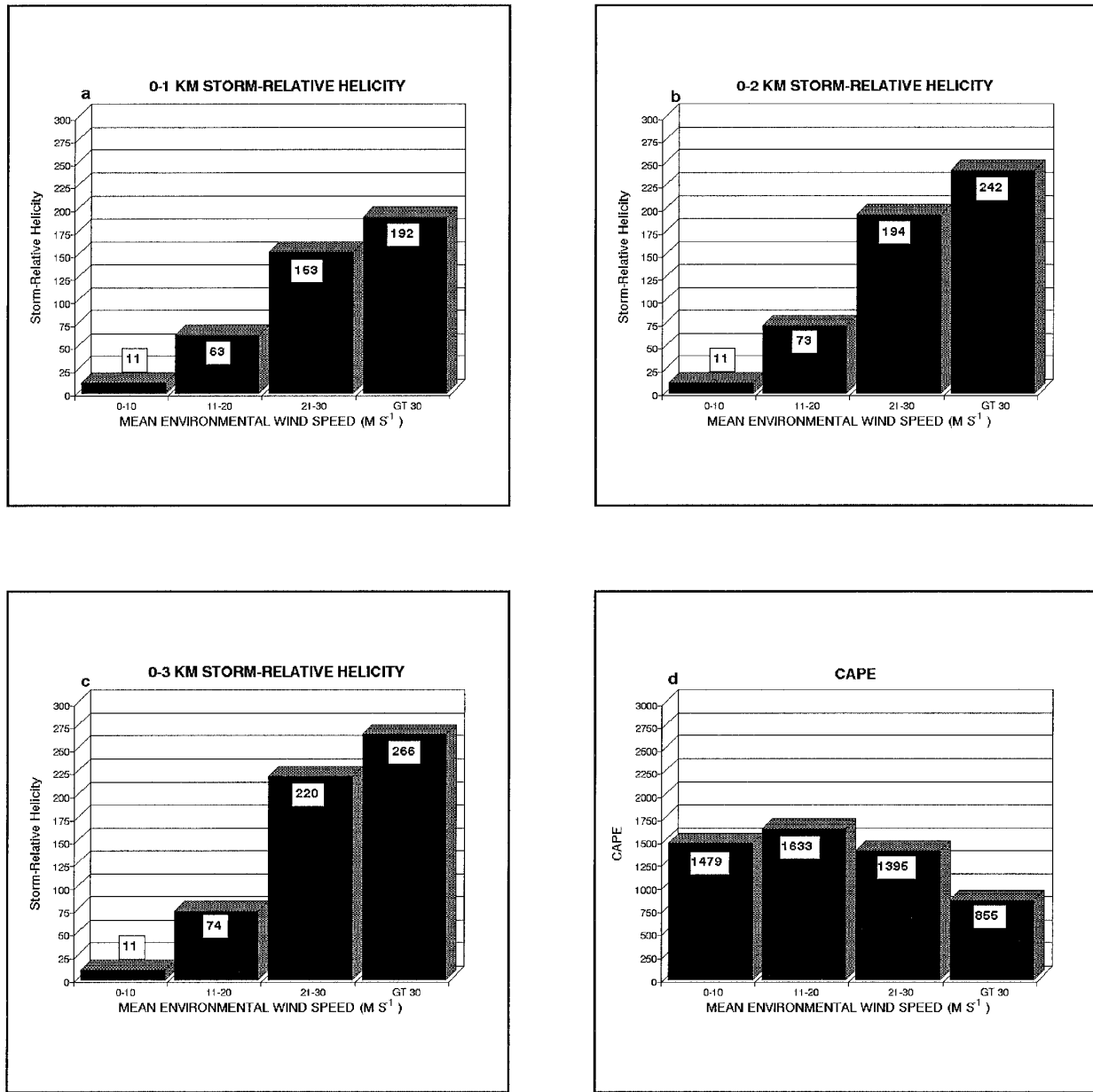
FIG. 12. As in Fig. 10 except for the mean environmental flow subsets.

(to a 99% confidence interval) by the chi-square statistic, χ^2, computed from the contingency table showing the distribution of F-scale intensity by CAPE (Table 2), as χ^2 is less than the value of $\chi^2_{0.01}$ for 6 degrees of freedom. Compare this result with those of similar tests conducted on the F scale versus 0–3-km storm-relative helicity (Table 3) and the F scale versus the strength of the mean environmental flow (Table 4), which indicate that F-scale intensity is dependent on the magnitude of both storm-relative-helicity and the mean environmental flow.

The preceding results imply that there is a preferred storm-relative flow structure for tornado-producing thunderstorms, independent of the thermodynamic environment as quantified by CAPE. This structure is consistent with that commonly associated with supercells (e.g., Browning 1964; Lemon

TABLE 1. Percentage of storm-relative winds within 40° of the mean storm-relative wind vector at their respective height AGL.

Mean environmental flow subset	F scale (avg)	Wind height			
		0.5 km	4 km	7 km	12 km
10 m s^{-1} or less	0.6	59%	66%	59%	41%
11–20 m s^{-1}	1.0	81%	22%	41%	41%
21–30 m s^{-1}	1.4	91%	54%	72%	70%
>30 m s^{-1}	1.9	96%	63%	79%	83%

and Doswell 1979; Klemp 1987; Droegemeier et al. 1993; and Brooks et al. 1994a,b). Furthermore, *given the occurrence of a tornadic supercell,* tornadic intensity appears to be linked to the strength of the storm-relative helicity *and the magnitude of the storm-relative winds at all levels,* as flow veers with height from the right-front storm quadrant to the rear of the storm in the upper troposphere.

e. Storm motion with respect to the mean environmental wind

Much research has been devoted to storm propagation and its tendency to deviate from the mean envi-

ronmental flow in which it is embedded (e.g., Browning 1964). In the manner of Darkow and McCann (1977), the dataset was subdivided according to storm motion with respect to mean environmental wind direction. Storms moving 15° or more to the left of the mean wind were classified as left-moving storms (22 cases), while those moving 15° or more to the right of the mean wind were classified as right-moving storms (74 cases). All others were categorized as storms in the direction of the mean environmental wind, a subset comprising nearly one-half the database, with 85 storms exhibiting little deviate motion.

The most obvious difference among these subsets (presented in Fig. 14) is shown to be associated with the direction toward which the upper flow impinges upon the updraft. Upper-level storm-relative flow is sharply focused on the right-rear storm quadrant for right-moving storms and to the immediate rear of the storm for the mean movers, while it is more broadly focused on the left-rear quadrant for left-moving storms.

With low-level inflow averaging less than 10 m s^{-1}, and approaching the right-front storm quadrant in the lowest kilometer, the mean profile for the left-moving storms is *not* clearly typical of those associated with anticyclonically rotating left-moving supercells (e.g.,
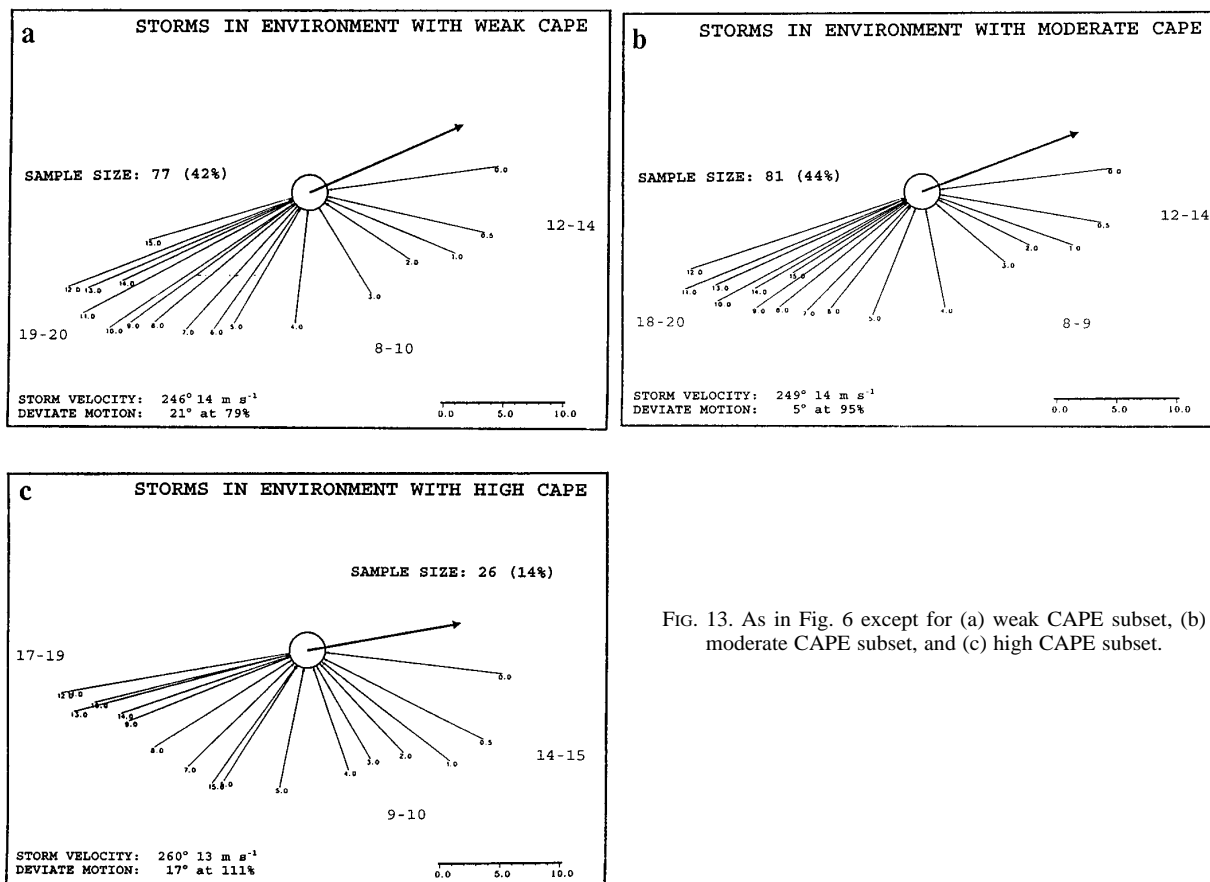

FIG. 13. As in Fig. 6 except for (a) weak CAPE subset, (b) moderate CAPE subset, and (c) high CAPE subset.

TABLE 2. Distribution of F-scale intensity by CAPE for the 184 tornadic storms composing the database in this study. Expected frequencies are shown in parentheses. $\chi^2 = 6.65 < 16.81$, the value of $\chi^2_{0.01}$ for 6 degrees of freedom.

	F scale				
CAPE	F-0	F-1	F-2	F-3/F-4	Totals
Weak	19 (20.1)	33 (31.0)	22 (18.4)	3 (7.5)	77
Moderate	21 (21.1)	32 (32.6)	17 (19.4)	11 (7.9)	81
High	8 (6.8)	9 (10.5)	5 (6.2)	4 (2.5)	26
Totals	48	74	44	18	184

TABLE 3. As in Table 2 except for F-scale vs 0–3-km storm-relative helicity (absolute value of, in $m^2\ s^{-2}$); $\chi^2 = 30.1 > 16.81$, the value of $\chi^2_{0.01}$ for 6 degrees of freedom.

S–R	F scale				
helicity	F-0	F-1	F-2	F-3/F-4	Totals
< =50	25 (14.9)	24 (22.9)	7 (13.6)	1 (5.6)	57
50–150	15 (14.1)	24 (21.7)	10 (12.9)	5 (5.3)	54
>150	8 (19.0)	26 (29.4)	27 (17.5)	12 (7.1)	73
Totals	48	74	44	18	184

Browning 1964; Klemp and Wilhelmson 1978; Droegemeier et al. 1993). Further evidence of this is provided by storm-relative helicity values (Figs. 15a–c), which suggest little preferred sense of anticyclonic updraft rotation. The mean environmental wind profile for these storms (not shown) possesses a hodograph with cyclonic curvature and weak to moderate shear through the lowest several kilometers, while the mean CAPE is nearly the same as that of the right-moving storms (Fig. 15d). This environment is comparable to the environment numerically simulated by Weisman and Klemp (1984), which supported coexisting, but dynamically distinct, left- and right-moving (with respect to the mean shear vector of the 0–6-km layer) storms. While right-moving convection was found to be supercellular in nature, left-moving convection was multicellular, with dominant forcing provided by low-level convergence associated with the downdraft outflow.

The mean storm-relative wind profiles for both the mean- and right-movers is consistent with conceptualizations of supercells. Strong low-level flow approaches the right-front storm quadrant, veering significantly with height through the lowest several kilometers. Helicity values in the 0–1-km layer are very similar for the two subsets, but it becomes apparent that right-moving storms possess greater storm-relative helicity values through deeper layers of the lower troposphere.

4. Summary and concluding statements

The tornado proximity sounding collection examined in this study is believed to be the largest, most restrictive dataset of its kind, which includes radar observed storm velocities and contains a representative sampling of all tornado occurrences throughout the contiguous United States east of the Rockies. Mean storm-relative wind profiles were derived for a data sample of 184 tornado-producing thunderstorms and numerous sample subsets based on tornadic intensity, strength of the mean environmental flow, magnitude of CAPE, and direction of storm motion with respect to the mean environmental wind vector.

Despite the broad range of environmental conditions exhibited by the data, the mean profiles suggest that there is a preferred storm-relative flow structure for tornadic thunderstorms, one independent of the thermodynamic environment and consistent with conceptual models of supercells. While mid- and upper-level storm-relative winds display considerable directional variability on the right and rear updraft flanks, low-level storm-relative winds are much more consistent in their approach on the right-front storm quadrant, with a substantial component of vorticity in the streamwise direction (storm-relative helicity averages 142 $m^2\ s^{-2}$ in the surface to 3-km layer). Tornadic intensity in association with these storms appears to strengthen as 1) the magnitude of storm-relative helicity grows through an increasingly deep layer and 2) mid- and upper-level storm-relative winds strengthen and possess decreasing directional variability.

It was pointed out by Brooks et al. (1994a) that the impact of mid- and upper-tropospheric environmental wind fields on convection has been somewhat overlooked in recent years, as researchers have focused almost exclusively on the lower levels of the

TABLE 4. As in Table 2 except for F-scale vs strength of mean environmental flow (in $m\ s^{-1}$); $\chi^2 = 33.8 > 21.7$, the value of $\chi^2_{0.01}$ for 9 degrees of freedom.

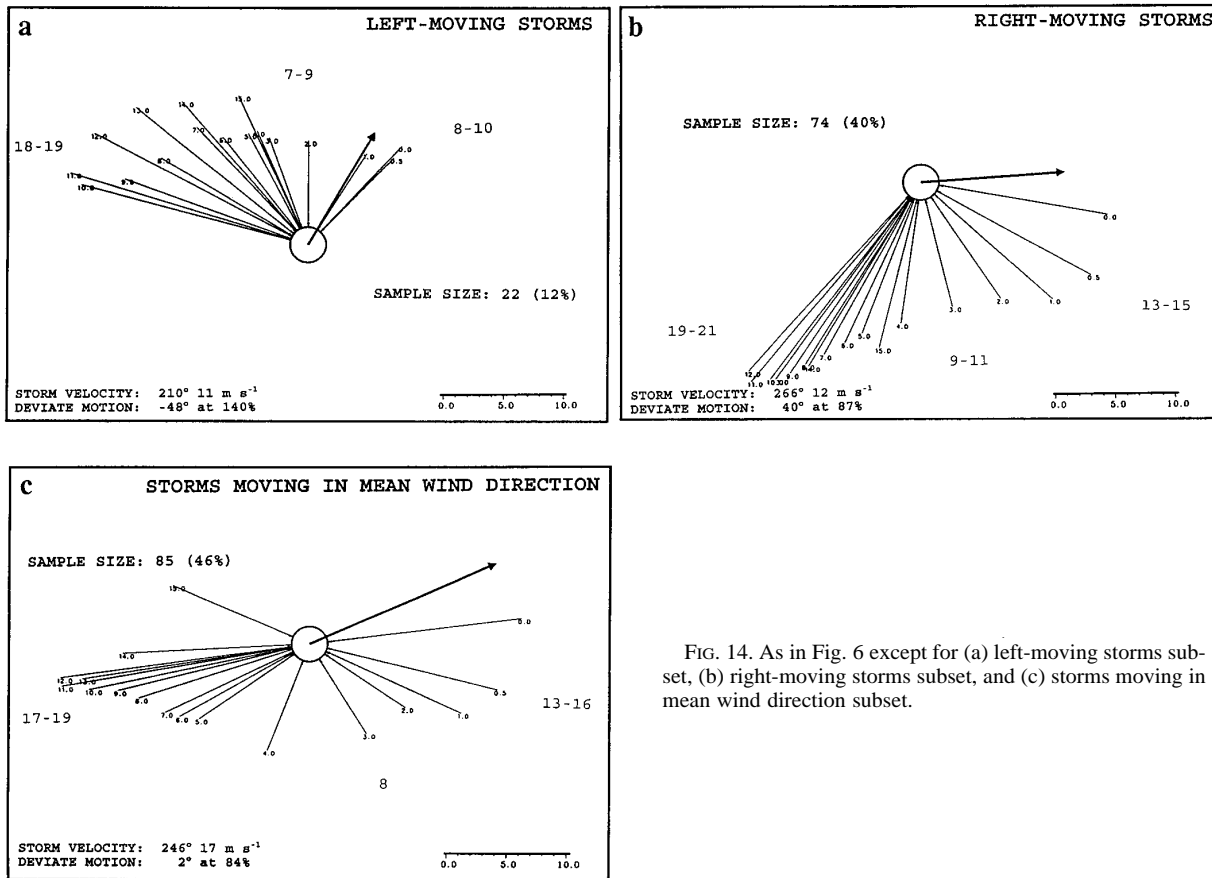| Mean	F scale				
flow	F-0	F-1	F-2	F-3/F-4	Totals
< =10	16 (7.6)	10 (11.7)	3 (6.9)	0 (2.8)	29
11–20	16 (16.7)	32 (25.7)	13 (15.3)	3 (6.3)	64
21–30	15 (17.5)	25 (26.9)	17 (16.0)	10 (6.6)	67
>30	1 (6.3)	7 (9.7)	11 (5.7)	5 (2.3)	24
Totals	48	74	44	18	184

FIG. 14. As in Fig. 6 except for (a) left-moving storms subset, (b) right-moving storms subset, and (c) storms moving in mean wind direction subset.

hodograph. Observational evidence, however, suggests that the influence of flow at these levels (7–12 km) should not be underestimated. Contributing significantly to storm propagation, mid- and upper-level environmental wind fields can be critical to the strength of the low-level storm-relative flow and storm-relative helicity, in addition to the strength and orientation of the mid- and upper-level storm-relative winds.

As suggested by Wakimoto and Wilson (1989), it is apparent that a number of tornadoes occur independent of the larger-scale flow, particularly in weak shear/weak environmental flow regimes often associated with nonmesocyclonic convection. This is well illustrated by the mean storm-relative wind profile for the 10 m s^{-1} or less mean environmental flow subset (Fig. 11a), which suggests little potential for either updraft rotation or the development of vertical perturbation pressure gradients supporting sustained updrafts.

Wakimoto and Wilson hypothesized that tornadogenesis in association with nonmesocyclonic convection occurs as boundary-layer-based vortices, generated by shearing instabilities along low-level convergence boundaries, intensify due to vertical stretching beneath strengthening updrafts. Interestingly, they further proposed that this same low-level vortex spinup process could explain tornadogenesis in supercells and, through interaction with the mesocyclone, may account for the development of strong and violent tornadoes. Although the primary mechanism by which the low-level pretornadic circulation develops in supercells has yet to be resolved (assuming there is a ''primary'' mechanism), the conceptual models of Klemp and Rotunno (1983), Wakimoto and Wilson (1989), and Davies-Jones and Brooks (1993) all stress that this vortex is strongly amplified by intense vertical stretching in the vicinity of the updraft. This concept of ''vortex stretching'' seems to be supported by the F-scale subsets and the mean environmental flow subsets presented in this paper, as tornadic intensity increases with storm-scale dynamic forcing associated with strengthening updraft rotation and an increasingly favorable vertical perturbation pressure gradient through a deep portion of the cloud-bearing layer on the inflow side of the updraft.
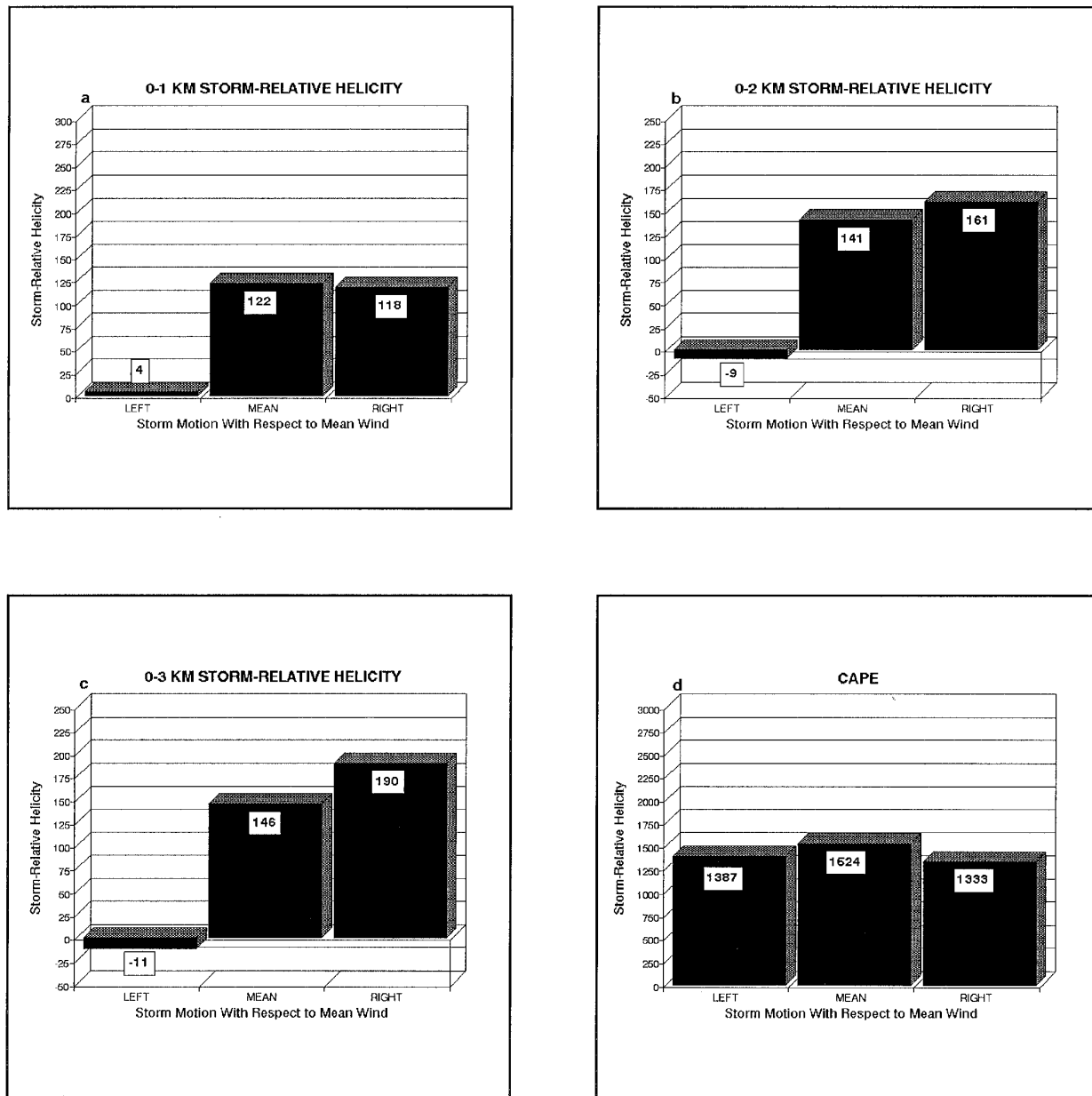
FIG. 15. As in Fig. 10 except for direction of storm motion with respect to the mean environmental wind subsets.

REFERENCES

Beebe, R. G., 1955: Types of airmasses in which tornadoes occur. *Bull. Amer. Meteor. Soc.,* **36,** 349–350.

Brooks, H. E., C. A. Doswell III, and R. B. Wilhelmson, 1994a: The role of midtropospheric winds in the evolution and maintenance of low-level mesocyclones. *Mon. Wea. Rev.,* **122,** 126–136.

——, ——, and J. Cooper, 1994b: On the environments of tornadic and nontornadic mesocyclones. *Wea. Forecasting,* **9,** 606–618.

Browning, K. A., 1964: Airflow and precipitation trajectories within severe local storms which travel to the right of the mean winds. *J. Atmos. Sci.,* **21,** 634–639.

Byers, H. R., and R. R. Braham Jr., 1949: *The Thunderstorm.* U.S. Government Printing Office, 287 pp.

Carbone, R. E., 1983: A severe frontal rainband. Part II: Tornado parent vortex circulation. *J. Atmos. Sci.,* **40,** 2639–2654.

Darkow, G. L., 1969: An analysis of over sixty tornado proximity soundings. Preprints, *Sixth Conf. on Severe Local Storms,* Chicago, IL, Amer. Meteor. Soc., 218–221.

——, and D. W. McCann, 1977: Relative environmental winds for 121 tornado bearing storms. Preprints, *10th Conf. on Severe Local Storms,* Omaha, NE, Amer. Meteor. Soc., 413–417.

Davies-Jones, R. P., 1984: Streamwise vorticity: The origin of updraft rotation. *J. Atmos. Sci.,* **41,** 2991–3006.

——, and H. E. Brooks, 1993: Mesocyclogenesis from a theoretical perspective. *The Tornado: Its Structure, Dynamics, Prediction, and Hazards, Geophys. Monogr.,* No. 79, Amer. Geophys. Union, 105–114.

——, D. W. Burgess, and M. Foster, 1990: Test of helicity as a tornado forecast parameter. Preprints, *16th Conf. on Severe Local Storms,* Kananaskis Park, AB, Canada, Amer. Meteor. Soc., 588–592.

Doswell, C. A., III, and D. W. Burgess, 1993: Tornadoes and tornadic storms: A review of conceptual models. *The Tornado: Its Structure, Dynamics, Prediction, and Hazards, Geophys. Monogr.,* No. 79, Amer. Geophys. Union, 161–172.

Droegemeier, K. K., S. M. Lazarus, and R. Davies-Jones, 1993: The influence of helicity on numerically simulated convective storms. *Mon. Wea. Rev.,* **121,** 2005–2009.

Fawbush, E. J., and R. C. Miller, 1954: The types of air masses in which North American tornadoes form. *Bull. Amer. Meteor. Soc.,* **35,** 154–165.

Fujita, T. T., 1971: A proposed characterization of tornadoes and hurricanes by area and intensity. SMRP Res. Paper 91, Dept. of Geophysical Sciences, University of Chicago, 42 pp.

Johns, R. H., and C. A. Doswell III, 1992: Severe local storms forecasting. *Wea. Forecasting,* **7,** 588–612.

Klemp, J. B., 1987: Dynamics of tornadic thunderstorms. *Annu. Rev. Fluid Mech.,* **19,** 369–402.

——, and R. Rotunno, 1983: A study of the tornadic region within a supercell thunderstorm. *J. Atmos. Sci.,* **40,** 359–377.

——, and R. B. Wilhelmson, 1978: Simulations of right- and left-moving storms produced through storm splitting. *J. Atmos. Sci.,* **35,** 1097–1110.

Lemon, L. R., and C. A. Doswell III, 1979: Severe thunderstorm evolution and mesocyclone structure as related to tornadogenesis. *Mon. Wea. Rev.,* **107,** 1184–1197.

Lilly, D. K., 1986a: The structure, energetics, and propagation of rotating convective storms. Part I: Energy exchange with the mean flow. *J. Atmos. Sci.,* **43,** 113–125.

——, 1986b: The structure, energetics, and propagation of rotating convective storms. Part II: Helicity and storm stabilization. *J. Atmos. Sci.,* **43,** 126–140.

Maddox, R. A., 1976: An evaluation of tornado proximity wind and stability data. *Mon. Wea. Rev.,* **104,** 133–142.

Newton, C. W., and H. R. Newton, 1959: Dynamical interactions between large convective clouds and environment with vertical shear. *J. Meteor.,* **16,** 483–496.

Ostby, F. P., 1993: The changing nature of tornado climatology. Preprints, *17th Conf. on Severe Local Storms,* St. Louis, MO, Amer. Meteor. Soc., 1–5.

Rotunno, R., 1981: On the evolution of thunderstorm rotation. *Mon. Wea. Rev.,* **109,** 577–586.

——, and J. B. Klemp, 1982: The influence of shear-induced pressure gradient on thunderstorm motion. *Mon. Wea. Rev.,* **110,** 136–151.

——, and ——, 1985: On the rotation and propagation of simulated supercell thunderstorms. *J. Atmos. Sci.,* **42,** 271–292.

Wakimoto, R. M., and J. W. Wilson, 1989: Non-supercell tornadoes. *Mon. Wea. Rev.,* **117,** 1113–1140.

Weisman, M. L., and J. B. Klemp, 1982: The dependence of numerically simulated convective storms on vertical wind shear and buoyancy. *Mon. Wea. Rev.,* **110,** 504–520.

——, and ——, 1984: The structure and classification of numerically simulated convective storms in directionally varying shears. *Mon. Wea. Rev.,* **112,** 2479–2498.

——, and ——, 1986: Characteristics of isolated convective storms. *Mesoscale Meteorology and Forecasting,* P. S. Ray, Ed., Amer. Meteor. Soc., 331–358.

Wilson, J. W., 1986: Tornadogenesis by nonprecipitation induced shear lines. *Mon. Wea. Rev.,* **114,** 270–284.